Lung infection segmentation for COVID-19 pneumonia based on a cascade convolutional network from CT images

Ramin Ranjbarzadeh[1], **Saeid Jafarzadeh Ghoushchi***[2] , **Malika Bendechache**[3] , **Amir Amirabadi**[4], **Mohd Nizam AB Rahman**[5], **Soroush Baseri Saadi**[6], **Amirhossein Aghamohammadi**[7], **Mersedeh Kooshki Forooshani**[8]

[1] Department of Telecommunications Engineering, Faculty of Engineering, University of Guilan, Rasht, Iran
ranjbar.ramin24@gmail.com

*[2] Faculty of Industrial Engineering, Urmia University of Technology, Urmia, Iran.
s.jafarzadeh@uut.ac.ir

[3] School of Computing, Faculty of Engineering and Computing, Dublin City University, Ireland.
malika.bendechache@dcu.ie

[4] Department of Electrical Engineering, Islamic Azad University, South Tehran Branch, Tehran, Iran.
a_amirabadi@azad.ac.ir

[5] Department of Mechanical and Manufacturing Engineering, Faculty of Engineering and Built Environment, Universiti Kebangsaan Malaysia, 43600 Bangi Selangor, Malaysia.
mnizam@ukm.edu.my

[6] Department of Electrical Engineering, Islamic Azad University, South Tehran Branch, Tehran, Iran.
soroushbaserisaadi@gmail.com

[7] Institute of Visual Informatics, Universiti Kebangsaan Malaysia, Bangi, Selangor, Malaysia.
amho.mohammadi@gmail.com

[8] Department of Electronics and Telecommunications, Polytechnic university, turin, Italy.
mersedeh_kooshki@yahoo.com

---

* corresponding author

Abstract

The COVID-19 pandemic is a global, national, and local public health which causing a significant outbreak in all countries and regions for both males and females around the world. Automated detection of lung infections and their boundaries from medical images offers a great potential to augment the patient treatment healthcare strategies for tackling COVID-19 and its impacts. Detecting this disease from lung CT scan images is perhaps one of the fastest ways to diagnose the patients. However, finding the presence of infected tissues and segment them from CT slices faces numerous challenges, including similar adjacent tissues, vague boundary, and erratic infections. To overcome the mentioned problems, we propose a two-route convolutional neural network (CNN) by extracting global and local features for detecting and classifying COVID-19 infection from CT images. Each pixel from the image is classified into normal and infected tissue. For improving the classification accuracy, we used two different strategies including Fuzzy c-mean clustering and local directional pattern (LDN) encoding methods to represent the input image differently. This allows us to find more complex pattern from the image. To overcome the overfitting problems due to small samples, an augmentation approach is utilized. The results demonstrated that the proposed framework achieved Precision 96%, Recall 97%, F-score, average surface distance (ASD) of 2.8 ± 0.3 mm and volume overlap error (VOE) of $5.6\pm1.2\%$.

Keywords: Deep learning, CNN, Lung infection, COVID-19, Lung segmentation

Introduction:

Since December 2019, the world has been experiencing a new coronavirus disease which can cause trigger asthma symptoms, acute respiratory illness pandemics in people of any age, and even permanent changes in the lungs' biology. This disease was reported first time in Wuhan, Hubei province of China, and became an epidemic all over the World (Shan et al. 2020; Jaiswal et al. 2020). The common symptoms of COVID-19 are short breathing, diarrhea, a cough, sore throat, a headache, and fever. Vanishing of taste, nasal blockage, loss of smell, aches, and tiredness can also be observed in patients. The new infectious diseases infected by the virus were named Coronavirus Disease 2019 (COVID-19) by World Health Organization (WHO) and this coronavirus was named as SARS-CoV-2 by the International Committee on Taxonomy of Viruses (ICTV) (Wang et al. 2020b; Ahmadi et al. 2020). As there is no definite vaccine available for prevention from COVID-19 and infectious disease everyone can be easily infected from other infected people. The only way for preventing the spread of virus infection in healthy persons is isolation. As there is not provided a vaccine or any cure for this virus so far, the best way is isolating peoples and diagnosis the infected person by any possible legal approach. One of the best methods is that looking at the obtained image from the chest of a patient using a screening method such as X-ray or CT images (Kamble, Sahu & Doriya 2020; Dorosti et al. 2020; Zhou et al. 2020).

Inflammation growths in the lung can pose significant risks to human health. The increasing occurrence of the infected people among the population needs to introduce a more efficient treatment along with a cost-effective procedure that relies on its primary diagnosis. Providing prompt and precise recognition of the infected tissue plays a key role in effective patient treatment and survival (Chen et al. 2020; Hamzenejad et al. 2020).

A CT scan or computed tomography scan as a routine tool and a high sensitivity for the diagnosis of COVID-19 is broadly employed in hospitals and can perform early screening for defected tissue to recognize them precisely (Shi et al. 2020; Rubin et al. 2020; Wang et al.

2020a). Doctors and specialists are increasingly employing such imaging modality to categorize local injuries and lesions (Ardakani et al. 2020). Also, due to intensity similarity between lesions and normal tissues in CT images, the precise detection and segmentation of the infected area are certainly a cumbersome task, even for experienced radiologists or doctors (Ranjbarzadeh & Saadi 2020; Fan et al. 2020). The flow of detection and feature extraction of texture information from the lung via manual observation is a time-consuming, tedious, and monotonous process. Computer-aided diagnostic (CAD) approaches are using for such tasks and are based on artificial intelligence and machine learning algorithms to recognize the border differences between two objects. These procedures are standardizable, reproducible, and can be useful in enhancing diagnostic accuracy in a very short time. These procedures acting by assisting doctors and experts to accomplish many sophisticated tasks more accurately employing a combination of diversity classification approaches with a practical running time (Ouyang et al. 2020; Ahmadi et al. 2020).

Image segmentation is a complex and challenging area of the biomedical engineering task that is affected by numerous aspects, including illumination, low contrast, noise, and irregularity of the objects. Segmentation refers to partition an image into various parts or regions based on similar characteristics in neighboring proximity.

Deep learning systems, as a prominent segment of the rising artificial intelligence (AI) technology in recent years, have been reported with significantly improved diagnostic accuracy in medical imaging(Shi et al. 2020; Rajinikanth et al. 2020). These intelligent systems are aiding an accelerated progress in early-stage diagnosis and treatment of many diseases including automatic detection of liver, lung, brain diseases (Ouyang et al. 2020). Therefore, the aim of our study is to develop a deep learning model for automatic diagnosis of regions of lungs infected with COVID-19 virus using chest CT volumes.

Minaee et al. (2020) investigated the application of deep learning structures on chest radiography images to detect COVID-19 patients. For this purpose, they employed four popular convolutional neural networks, including DenseNet-121, ResNet18, SqueezeNet, and ResNet50 to identify COVID-19 disease in the analyzed chest X-ray images. Also, transfer learning on a subset of 2000 radiograms was applied to all networks to overcome the overfitting problem and improve the models' accuracy. Fan et al. (2020) applied a Lung Infection Segmentation Deep Network (Inf-Net) for dividing the infected tissue in a CT slice automatically. In the first step, a parallel partial decoder is employed for aggregating the high-level features and create a global map. Then, to increase the accuracy, the implicit reverse attention and explicit edge-attention were incorporated into a model to segmentation the boundaries.

A 3D deep convolutional neural Network (DeCoVNet) proposed in (Wang et al. 2020b) for detecting COVID-19 from CT volumes. They used a pre-trained UNet model to generates the 3D lung masks. The proposed DeCoVNet was divided into three stages. The first stage is called the network stem, which consisted of a vanilla 3D convolution. A batch normalization layer and a pooling layer with a kernel size of 5×7×7 were used to preserve rich local visual information based on the ResNet (He et al. 2016a) and AlexNet (Krizhevsky, Sutskever & Hinton 2012). Also, two 3D residual blocks (ResBlocks) were employed in the second stage. Lastly, a progressive classifier (ProClf) was utilized.

Early phase detection of Coronavirus proposed by (Barstugan, Ozkaya & Ozturk 2020) which employed five different feature extraction algorithms. To classify the extracted features, Support Vector Machines (SVM) along with 10-fold cross validation during the classification process was applied.

To overcome the limitations of previous works, a new hybrid algorithm for finding the location and boundary of the infected tissue from clinical CT images which takes advantage of clustering, local descriptor, and convolutional neural network is introduced. It is broadly considered to be challenging to find the exact location of the lesions inside the lung and extract their borders precisely due to the impact of the COVID-19 which caused the much similar intensity values across the lung. The growing progress of deep learning in all areas of image processing was a great motivation for this study. This work is interested to investigate the power of a CNN model for detecting and segmenting the infected regions inside the lung due to the COVID-19.

2. Methodology

The remaining parts of this paper are organized as follows. In part 2.1, the Z-Score normalization technique is represented. In part 2.2, the fuzzy clustering method is described. In part 2.3, an LDN encoding approach is proposed. In part 2.4, the architecture of the CNN is demonstrated. In part 2.5, Our CNN pipeline is represented. The explanation of the dataset, evaluation metrics, and experimental results are clarified in section 3. Our structure is displayed in Fig. 1.

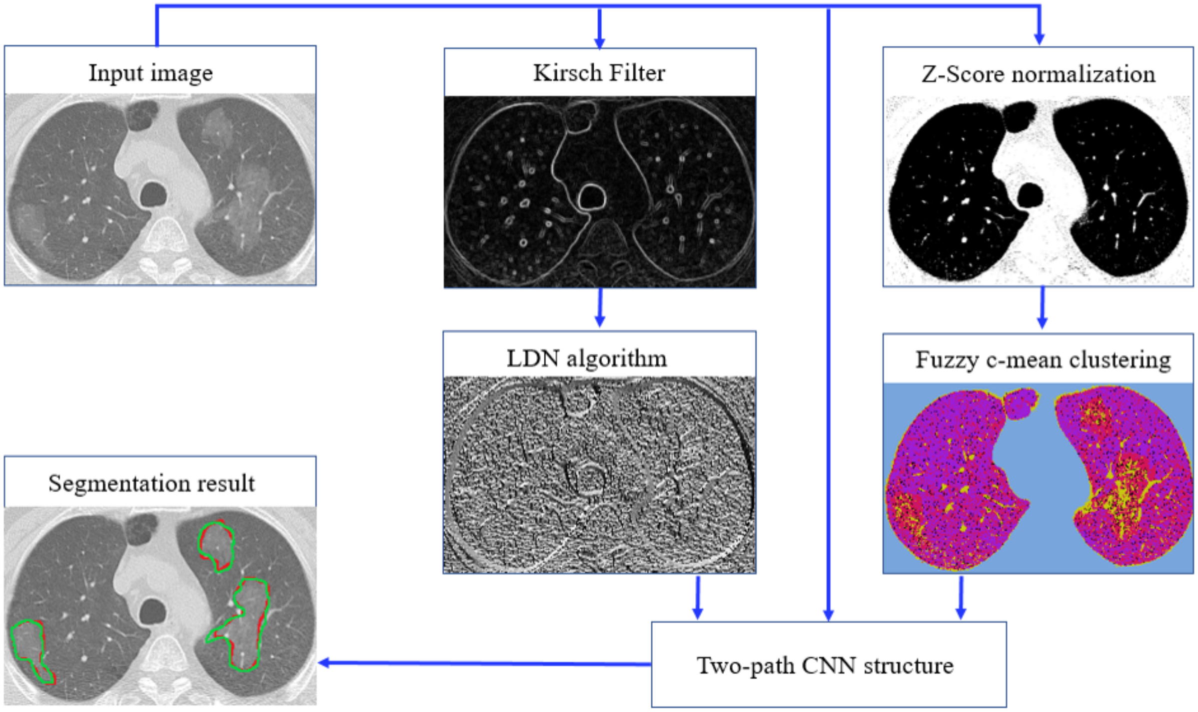

Fig. 1. Schematic of proposed pipeline for infected tissue segmentation.

2.1 Image normalization

As indicated in (Willner et al. 2015), due to the presence of the statistical noise in the computed tomography image (CT images) a deviation in the Hounsfield units (HUs) about a mean can be observed that lead to a high variance in gray scale or RGB values of all pixels in the image. These unwanted noises that affect the ability to visualize anatomic structures can be categorized into three main sources: 1) electronic noise that is an unwanted disturbance in an electrical signal caused by electrical equipment in the neighborhood. 2) noise of the reconstruction procedure due to imperfections in the receiver coils. 3) stochastic noise.

As the stochastic noise is the principal noise source in these kinds of imaging, the bad effects of it can be diminished in the imaging procedure by rising the quantity of photons (by considering a tradeoff between radiation risk and image quality). However, in obtained images from any Hospital or Medical Center, a significant amount of noise is observed which needs to be removed before starting the process of the segmentation.

By further investigation, we found out that a normalization approach can be beneficial to create a smooth image along with increasing the contrast of illumination near the border of the organs. So, to overcome the mentioned problems and enhance the result of the segmentation, a Z-Score normalization technique is employed so that all the non-zero values inside the image have unit variance and zero mean (Friedman & Komogortsev 2019; Khond 2020; Jafarzadeh Ghoushchi et al. 2020; Ghoushchi et al. 2020). Equation. 1 outlines how to apply the Z-Score normalization.

$$Z = (x - \mu)/\sigma \qquad (1)$$

where σ and μ indicate the standard deviation and mean value of non-zero pixels, respectively. Moreover, x describes the intensity of the current pixel.

Fig. 2. A demonstration of employing Z-Score normalization approach. a) Original images. b) Z-Score normalization.

The outcomes of the normalization strategy are depicted in Fig. 2. In Fig. 2, the first column shows the chest CT images of patients, and their corresponding lesions in the second column demonstrates the Z-Score output. As is illustrated in Fig. 2(b), the borders of both lungs are detected exactly without the effect of the lesions.

2.2 Fuzzy c-mean

After detecting the borders of the lungs with high accuracy, we need to recognize the volume and border of the infected areas inside the lungs more efficiently. The image of the detected lungs achieved from the previous stage has to be clustered to segment the infected areas from the other organs (background tissue). Clustering can be outlined as an unsupervised strategy that aims to fragment the input data (image or signal etc.) into the predefined segments (such as K-means method) or automated recognize parts (such as mean-shift method) based on certain criteria such as differences in the color, magnitude, and location (Bendechache, Le-Khac & Kechadi 2016; Bendechache, Kechadi & Le-Khac 2016; Bendechache 2019; Ranjbarzadeh & Baseri Saadi 2020). The fuzzy c-means (FCM) algorithm used in our work is an unsupervised data dividing/splitting strategy. In this method, data is split into n predefined natural groupings, namely, the so-called clusters such that every single pixel in the dataset be owned by at least two clusters with dissimilar weights. In this fuzzy partitioning technique, finding the cluster centre of each segment and related pixels are accomplished through an iterative optimization of the objective function (Bendechache & Kechadi 2015; Dhanachandra & Chanu 2020; Ranjbarzadeh, Saadi & Amirabadi 2020). This iterative optimization is accomplished by minimizing the following membership cost/objective function:

$$E = \sum_{k=1}^{m} \sum_{i=1}^{N} \mu_{ki} \| pixel_i - center_k \|^2 \tag{2}$$

$$\mu_{ki} = 1 \Bigg/ \left(\sum_{j=1}^{m} \left(\frac{pixel_i - center_k}{pixel_i - center_j} \right) \right)^{t}, \qquad \sum_{k=1}^{m} \mu_{ki} = 1, \quad \mu_{ki} \epsilon\, [0,1] \tag{3}$$

where $center_k$ shows the center of the kth cluster and $pixel_i$ illustrates the ith sample of I, μ_{ki} outlines the membership value of the ith sample with respect to the kth cluster which is linked inversely to the distance from $pixel_i$ to the cluster center $center_k$, m defines the number of clusters, t refers to the level of cluster fuzziness, N denotes the number of pixels inside the image I.

The result of the clustering on the lung's image is represented in Fig. 3. For better visualization, we applied a random value to each cluster in the RGB domain. As is illustrated clearly, by defining the number of five for the center of clusters by experimental results, a high distinction between the lesion and normal tissue can be observed in many samples. It means the number of clusters more or less than five cannot obtain an acceptable result. However, as depicted in Fig. 4, in some CT images due to much color similarity between the normal and lesion tissues, using only a clustering method to segment the lesions is not optimal. So, in the next step, textural analysis approaches will be employed to improve segmentation accuracy as much as possible.

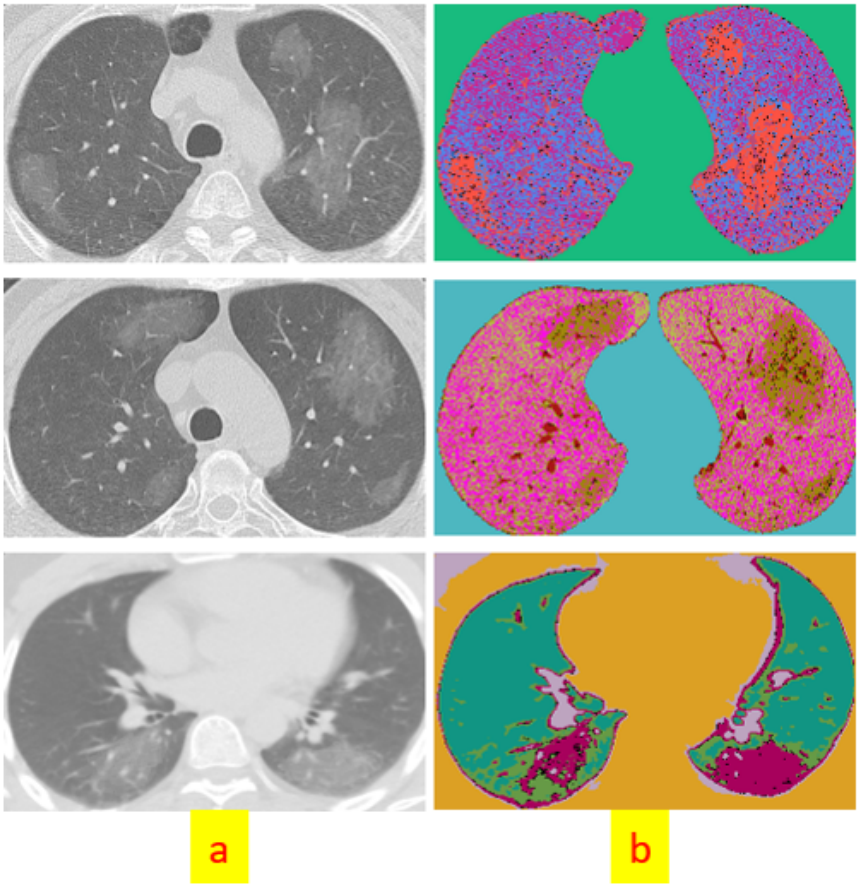

Fig. 3. A demonstration of employing Fuzzy c-mean clustering technique. a) Original images. b) Clustered images. For the better understanding, the colors of the clusters are in the RGB domain with random values.

2.3 Local Directional Number Pattern

Textural analysis of medical and biological images attempts to mine some characterizations of a surface texture such as smoothness, roughness, contrast, colors, and shapes (Tuncer, Dogan & Ozyurt 2020). As presented in many works (Leng et al. 2019; Naiemi, Ghods & Khalesi 2021), numerous types of local descriptors are used for converting images into a new representation based on the pre-defined coding rules or code-book of visual patterns.

Local Ternary Patterns (LTP) and Local Binary Pattern (LBP) feature descriptors are easy to implement and be influenced by the change of the pixel intensity of nearest-neighbor (circular, rectangular, etc. neighborhood) in clockwise or counter-clockwise to alter (encoding) the low-level information of a spot, edges, curve, and line inside an image and calculate the outcome as a binary value (Liu et al. 2016; Karimi, Ranjbarzadeh Kondrood & Alizadeh 2017). Owing to the robustness of the gradient value than a gray- level intensity in encoding applications, in recent investigations, some techniques based on the gradient value such as Local word directional pattern (LWDP) and local directional number patterns (LDN) have been attained much attention (Naiemi, Ghods & Khalesi 2021). The LDN operates in the gradient domain to create an illumination-invariant representation of the image. It uses directional information for recognizing edge locations that their magnitudes are insensitive to lighting variations.

In our work, the first phase for encoding the chest images is to define the location and value of all significant edges. This is implemented by operating the 8 directions Kirsch kernels (filters) that are rotated by 45° in the 8 main compass directions (Fig. 4). These non-linear edge detector kernels are responsible for identifying the final edges. Each filter produces a feature map and only the maximum value in each location is selected to create a final edge map (Luo et al. 2016; Uddin et al. 2017). An example of employing the non-linear kirsch filter to the chest images is depicted in Fig. 5. This section causes a substantial increase in final lesions segmentation, especially when the border of the lesions is vague.

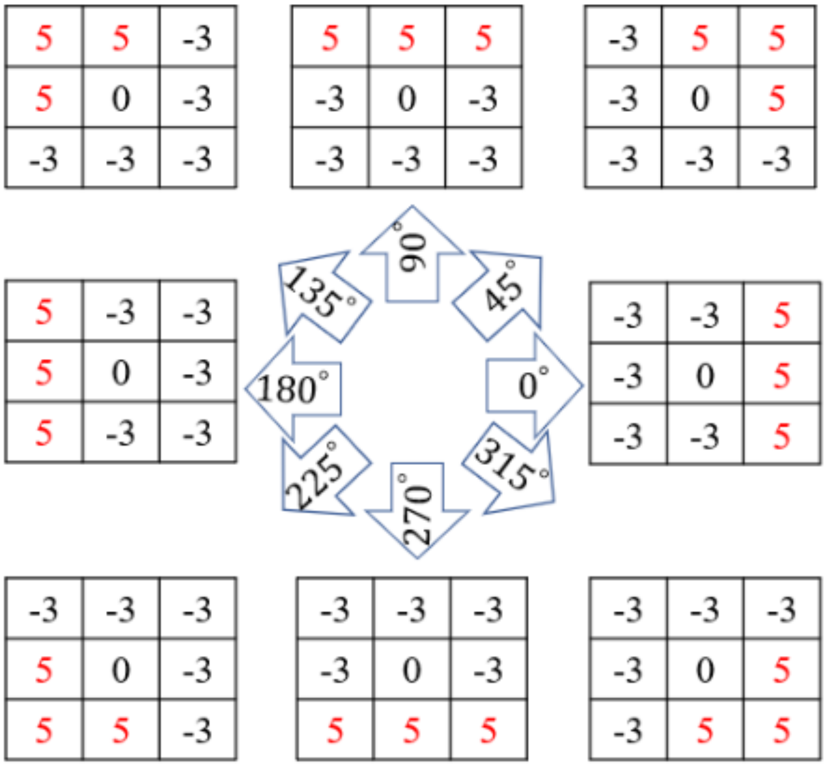

$$\begin{bmatrix} 5 & 5 & -3 \\ 5 & 0 & -3 \\ -3 & -3 & -3 \end{bmatrix} \quad \begin{bmatrix} 5 & 5 & 5 \\ -3 & 0 & -3 \\ -3 & -3 & -3 \end{bmatrix} \quad \begin{bmatrix} -3 & 5 & 5 \\ -3 & 0 & 5 \\ -3 & -3 & -3 \end{bmatrix}$$

$$\begin{bmatrix} 5 & -3 & -3 \\ 5 & 0 & -3 \\ 5 & -3 & -3 \end{bmatrix} \quad \begin{bmatrix} -3 & -3 & 5 \\ -3 & 0 & 5 \\ -3 & -3 & 5 \end{bmatrix}$$

$$\begin{bmatrix} -3 & -3 & -3 \\ 5 & 0 & -3 \\ 5 & 5 & -3 \end{bmatrix} \quad \begin{bmatrix} -3 & -3 & -3 \\ -3 & 0 & -3 \\ 5 & 5 & 5 \end{bmatrix} \quad \begin{bmatrix} -3 & -3 & -3 \\ -3 & 0 & 5 \\ -3 & 5 & 5 \end{bmatrix}$$

Fig. 4. Non-linear Kirsch kernels in 8 rotations (Ranjbarzadeh & Saadi 2020).

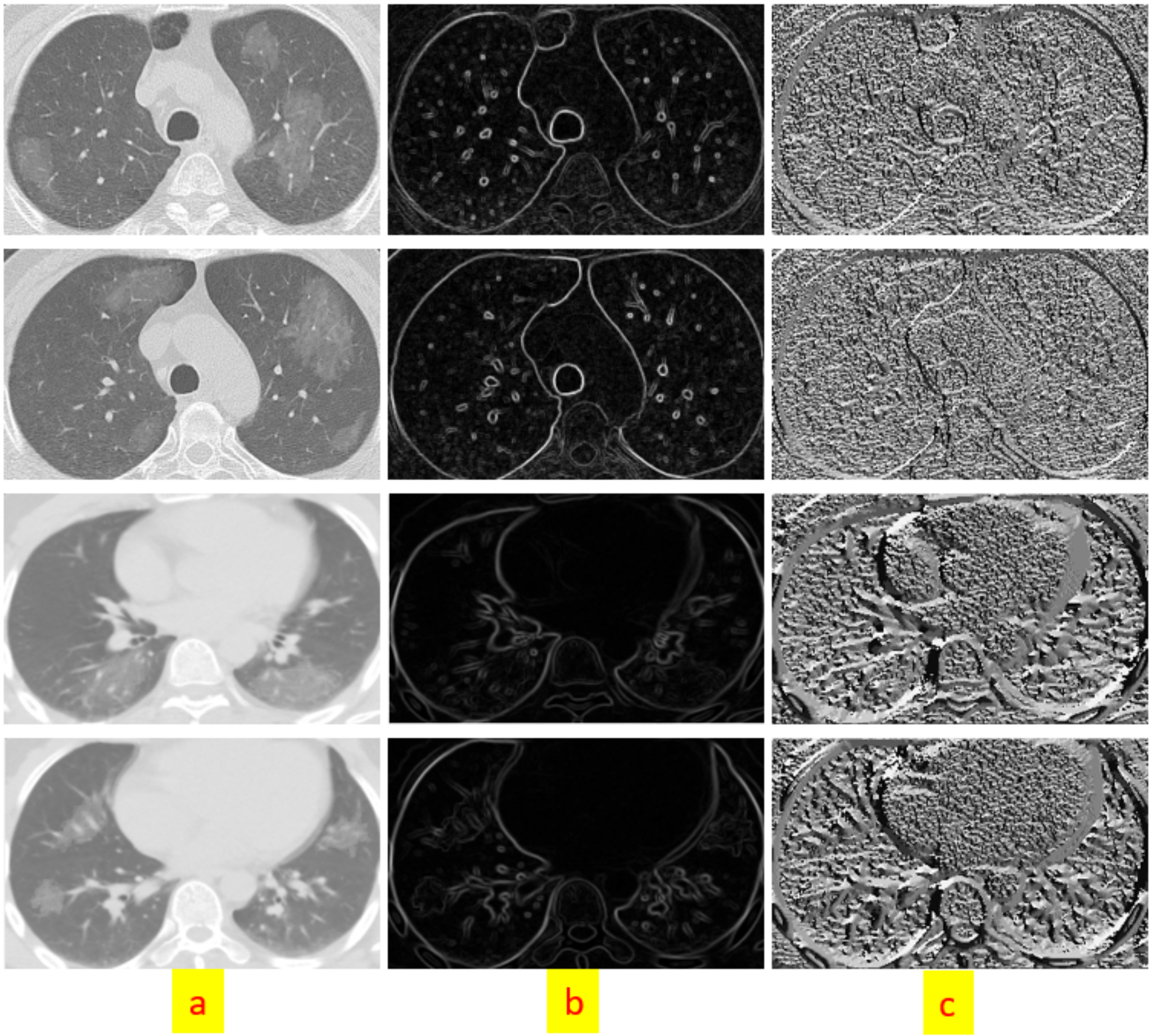

Fig. 5. The result of applying the kirsch filter and LDN approach to a chest image. The second column illustrates edge detection using the Kirsch filter. The third column demonstrates the results of the LDN technique.

2.4 Convolutional Neural Network Design

Automated recognition of patterns in data by computers based on knowledge already obtained or is called pattern recognition. It has applications in image analysis, information retrieval, signal processing, bioinformatics, data compression, statistical data analysis, computer graphics, and machine learning (Bendechache & Kechadi 2015; Bendechache 2019; de Assis Neto et al. 2020; Nasir et al. 2020; Azary & Abdoos 2020; Ranjbarzadeh, Baseri Saadi & Amirabadi 2020; Ali et al. 2020).

In machine learning approaches and applications, the convolutional neural network (CNN) structures demonstrate a high capability to extract and classify some key features and bridging the gap between the capabilities of machines and humans (Jafarzadeh-Ghoushchi & Rahman 2016; Islam, Islam & Asraf 2020; Waleed Salehi, Baglat & Gupta 2020). The structure of a CNN was inspired by the organization of the Visual Cortex in the Human Brain and is similar to that of the connectivity pattern of Neurons. Every neuron responds to irritant only in a constrained region of the visual field known as the Receptive Field. The CNN structure that originally designed for image analysis largely exploits the low-level and high-level of the textural features and is used in many applications including action detection and automated lesion segmentation (Mahmood et al. 2017; Hassantabar, Ahmadi & Sharifi 2020).

This neuron-based pipeline that captures temporal and spatial dependencies has a grid-like topology and permits us for extracting characteristics powerfully from the 1D or 2D input data by passing through a stack of convolution layers with the predefined dimension of the filters (Ucar & Korkmaz 2020; Nour, Cömert & Polat 2020; Naiemi, Ghods & Khalesi 2021). This grid-like model is a class of deep learning networks and have numerous trainable biases and weights based on the type of the topology and is applied for feature extraction, regression, and classification. These trainable weights need to be defined randomly at the beginning.

This structure is able to extract high-level features automatically from raw input features, which are considerably powerful than human-designed features. The core building block of a CNN is outlined as the convolutional layer which calculates the dot-product between input data and a set of learnable filters, much like a traditional neural network (Yin et al. 2016; Mahmood et al. 2017; Chen et al. 2018; Zhong et al. 2019). It should be noticed that the dimension of the filters is smaller than the dimension of the input data (Bengio 2012; Mahmood et al. 2017). The computed feature maps using the convolutional layer are achieved by stacking the activation maps of all kernels along the depth dimension. The output of one kernel (filter) applied to the previous layer is called the feature map. In the convolving process, for controlling the dimension of the feature maps, padding the input data with zeros around the border can be employed.

Mostly, the Spatial-Temporal dependencies at various scales are able to effectively obtain by the convolutional layers. The dimension of the kernel which defines the dimension of the receptive field needs to be selected based on the depth of the applied 1D, 2D, or 3D data. Also, stride defines how much the convolution filter can be moved at each step. Moreover, the bigger strides lead to less overlap between the receptive fields (smaller feature map) (Bengio 2012).

The high-level features are extracted (such as hand, legs, and, body in pedestrian detection) in the deeper convolutional layers of the model, while the first convolutional layers are responsible for mining the low-level information including curves, edges, and points. It should be mentioned that the numbers of columns and rows for each filter need to be an odd number, for instance, 9× 9, 7×7, and 3× 3 (Zhong et al. 2019).

It is noteworthy that the dimension of the extracted features in the last convolutional layer is greatly smaller than the input matrix (1D or 2D matrix). The diminution in the width and height of the image relies upon the length of the strides and the filter size employed for the convolution procedure.

The output of the convolution layer is fed to the activation layer in order to help the network learn complex patterns (Torres et al. 2018). This layer leaves the size of the applied matrix (data) unchanged. To decrease the consequence of the vanishing gradient in the training process, an activation function is utilized for each feature map to improve the computational effectiveness by inducing sparsity (Bengio 2012; Dolz, Desrosiers & Ben Ayed 2018).

In this study, the Non-Linearity (ReLU) activation function has been employed to shift the negative values to zero. The ReLU act as a linear function for positive and zero value. As all negative values change to the zero number, it leads some nodes to completely die and not learn anything. It means fewer neurons in the model would activate because of the limitations imposed by this layer.

Some of the most important benefits of the ReLU layer can be expressed as (Dureja & Pahwa 2018; Calik, Belen & Mahouti 2020; Schmidt-Hieber 2020):

1. Train Deep Networks: the architecture with large labeled datasets is able to reach to the best performance on purely supervised tasks.
2. Linear Behavior: The procedure of decreasing the cost function (optimization) in the CNN is much easier if their behavior could be close to a linear manner.
3. Representational Sparsity: As the ReLU layer shift the negative input values to the zero values, it causes some of the neurons in the hidden layers in neural networks to have zero values. In other words, by removing the effect of some neurons with zero weight an accelerating in the learning process can be achieved which is called a sparse representation.
4. Computational Simplicity: Dissimilar to the tanh and sigmoid activation functions, ReLU consists of only simple operations in terms of computation so that computing the exponential function in activations can be eliminated and therefore much more practicable to implement in models.

The ReLU layer does not cause the Vanishing Gradient Problem and avoid easy saturation. Also, due to overcoming the vanishing gradient issue, permitting models to learn faster and perform better. Equation (2) outlines how the ReLU activation function accomplishes (Dureja & Pahwa 2018; Calik, Belen & Mahouti 2020).

$$f(x) = \max(0, x) \tag{4}$$

where x demonstrates the input value and $f(x)$ is its related output.

Since in object recognition applications, there is evidence that demonstrates the form, dimension, color, or position of the object has no matter, and only the spatial variances need to be investigated. In order to accomplish this, a downsampling layer is applied by summarizing the key information in patches of each feature map without losing any details that lead to a good classification. In contrast to the convolution operation, the pooling layer has no parameters and only slides a window over its input, and simply takes the predefined value (mean, max, etc.) in the window. Furthermore, as the quantity of pixels in this layer (in both row and column) is dropped, leads to shortening the training time and combats overfitting (Di Cataldo & Ficarra 2017; Dong et al. 2018; Liu et al. 2019; Zhong et al. 2019).

An appropriate technique for dimensionality reduction of feature maps is to reduce the number of parameters and computation in the network so that the model can be robust to alter the high-frequency information (key information) and preserves vital features (Bengio 2012). This dimension-reduction procedure happens by utilizing a filter along the spatial dimensions (width, height) with a predefined dimension. This layer is regularly incorporated between two sequential convolutional layers. The max-pooling layer is accomplished in this study which first partitions the extracted matrix of features into a set of parts with no overlapping and then takes the maximum number inside each district. The max-pooling strategy also employs as a noise suppression technique (Yin et al. 2016; Doğantekin et al. 2019).

In a CNN structure (shallow or deep CNN), since the receptive field in the last convolutional layer does not cover the entire spatial dimension of the image, the generated features by the last convolutional layer correspond to a section of the input image. Therefore, one or some FC layers are obligatory in such a scenario. A Fully-Connected layer (FC) allows the model to learn the non-linear combinations of the high-level features in an input image.

Each node in the fully connected layer produces a single output with its learnable corresponding weight that is linked to all the activations in the previous nodes (Torres et al. 2018). It is noteworthy that before applying the generated feature matrixes to the fully connected layer, all 2D features have to be changed into a one-dimensional matrix (1D vector) (Rouhi et al. 2015b; Liu, Lin & Shen 2015; Ettensperger 2020). The latest layer for classification tasks in a CNN-based pipeline is the Softmax regression layer which is able to differentiate one from the other. The Softmax regression is also called Multinomial Logistic, Multi-class Logistic Regression, or just Maximum Entropy Classifier. This single-layer regression tries to normalize an input value into a vector of values to demonstrate how likely the input data belongs to a user-defined class. Also, as the output values are between the range [0,1], the sum of the output values obtained from the probability distribution procedure is equal to one (Rouhi et al. 2015a; Yin et al. 2016; Havaei et al. 2017; Chen et al. 2018).

For the training step, since we are not working with a big dataset with hundreds of different samples from many patients, it is enormously easy for the CNN-based models to converge or to be specialized according to its reliability level and application area (to be less intelligent). To overcome this issue, there are two main strategies: 1) transform learning. 2) data augmentation.

The transform learning method is utilized to bring some trained biases and weights into any pipeline rather than select them randomly at the first step. Data augmentation is a popular method for artificially boosting the number of training examples (He et al. 2016b; Dvornik, Mairal & Schmid 2019).

2.5 Our CNN pipeline

As mentioned before, CNNs are used to explore significant details from an input raw pixels more efficiently. Hence, in this study, we investigated the probability of the presence of the lesions caused by CVOID-19 using a novel model based on the combination of global and local features. Moreover, to maximize the segmentation accuracy for even small damaged healthy tissue, the proposed approach concludes three distinct input images instead of a single one. The three input images including original image, fuzzy clustered image, and encoded image (LDN). These three different inputs enable our model to handle many types of variability in the raw input pixels. The flowchart of the proposed structure is shown in detail in Fig. 6.

When we use CNNs for automatic feature extracting that are effective for various tumor or lesion detection problems, the need for preprocessing and highlighting the suspect regions is significantly reduced. This is due to the fact that the CNN-based structures have millions of parameters that are able to produce the best-suited feature maps for expressing the class probability. Although numerous CNN pipelines have been recommended for lesion segmentation in recently published papers, none of them has concentrated on applying the combined the textural encoding algorithm, fuzzy clustered, and raw image pixels as an input to a CNN structure. Since miscellaneous texture or images definitely encompass complementary and detailed information (features), our experimental outcomes for small samples (data) imply that this complex two-path strategy is effective to enhance the score of the evaluation indexes.

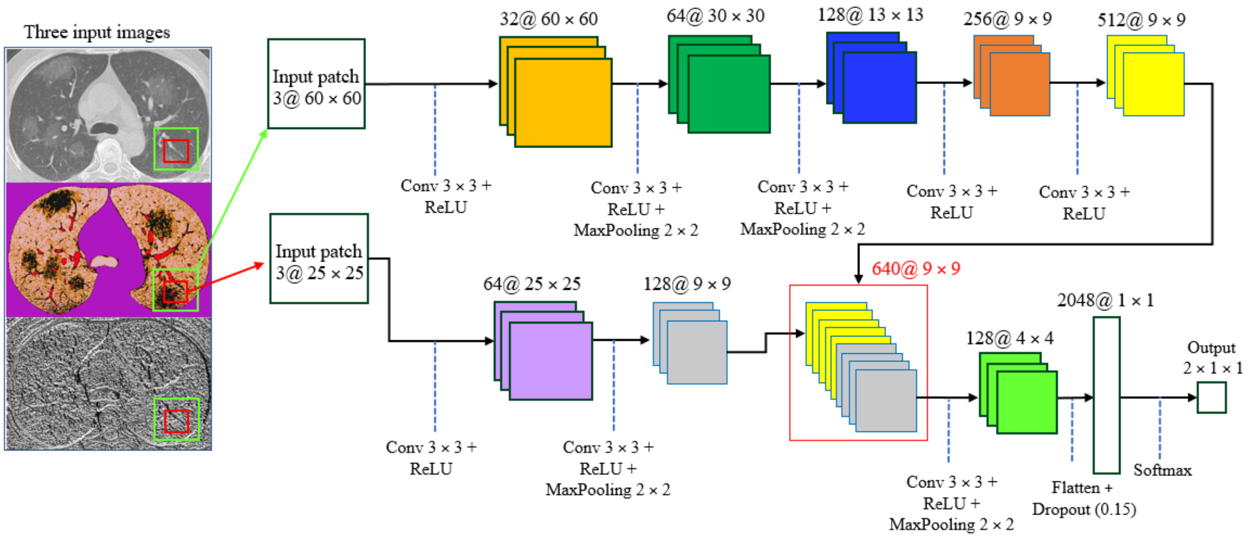

Fig. 6. Our implemented two-path CNN model using three distinct inputs.

To analyze the complex texture of our input images, due to many similarities of the lesion (infected area) with normal tissue in the margin of the lesion, semi-global and local features must to be taken into account. Moreover, the lesions may appear anywhere on the lung since COVID-19 has a multifocal distribution that for gaining better results need to have knowledge of neighbor information in a little further of each analyzing pixel location. As is clearly indicated in Fig. 6, the recommended cascading model is based on investigating key features using two distinct local and global paths.

In contrast to some other recently published methods such as (Hu et al. 2020), (Wang et al. 2020b), and (Fan et al. 2020) that employ all pixels inside the image as an input, our method only considers two patches from each applied 2D data (totally 6 patches) as an input to classify each pixel inside the output image. In other words, if there are 1000 pixels inside the image, the number of the produced patches are 1000×2, and due to the use of the three input images, there are 1000×2×3 patches. This is very interesting that using both local and global patches with a different route for extracting features can get better results compared to using only one of them.

In our model, two distinct routes are employed; the first one (upper path) comprises of the five convolutional layers for extracting the global features. The other path (bottom path) utilizes two convolutional layers for extracting the local features. The local and global investigation windows (patches) are 25×25 and 60×60, respectively.

The semi-global patches are employed for providing key details about the analogous touching textures with scar tissues, whilst the local patches are applied more for recognizing inflammation in the tiny air sacs. Moreover, the outcome of our strategy for inflammation detection highly depends on information extracted from the global windows. In Table 1, we exhibit the effect of employing semi-global and local patches in the ultimate outcome of our approach. As is depicted in Table 1, the best-observed dice score is obtained when the sizes of the local and global patch are 25×25 and 60×60, respectively.

Table 1. Investigating the accuracy of employing dissimilar dimensions of the regions in the final result of the approach.

Size of the semi-global patch	Size of the local patch	DICE value for lesion segmentation
40×40	11×11	24 %
50×50	11×11	31 %
60×60	11×11	33 %
70×70	11×11	40 %
80×80	11×11	41 %
40×40	15×15	61 %
50×50	15×15	70 %
60×60	15×15	72 %
70×70	15×15	73 %
80×80	15×15	81 %
40×40	21×21	74 %
50×50	21×21	76 %
60×60	21×21	81 %
70×70	21×21	88 %
80×80	21×21	91 %
40×40	25×25	56 %
50×50	25×25	73 %
60×60	**25×25**	**92 %**
70×70	25×25	89%
80×80	25×25	87 %

The size of the local region is 25×25×3, which three implies three distinct input images. The selected regions are convolved using 64 kernels to generate the feature maps based on the 3×3 receptive field. In the next layer, the number of filters is changed to 128 with the same receptive field. After producing feature maps in the first layer, the max-pooling layer is not used whilst after the second layer, max-pooling decrease the dimension of the produced feature maps.

Unlike the local features extraction path, in the global feature extraction procedure, five convolutional layers are employed. In this path, only two intermediate layers are employed that are using the max-pooling approach. All extracted feature maps with the size of 9×9 at the end of each route are concatenated to create 384 feature maps in order to use in the next convolutional layer. After the concatenation step, 128 kernels are applied to these feature maps, and then a max-pooling layer changes the all dimensions to the 4×4. Then, all created feature maps are transformed into a 2048×1 feature vector. Lastly, by applying a Softmax layer all extracted data are tagged to one of two expected classes (1 implies the inflammation and 2 shows the normal tissues.).

For minimizing the cross-entropy loss, the proposed CNN structure with two routes was learned through stochastic gradient descent (SGD) in 1,000 epochs with a batch size of 128(Wahab, Khan & Lee 2017), in Eq. (5). Our pipeline calculates the discrepancy between the predicted output and ground-truth for lesions segmentation. The dropout is applied before the FC layer, which is aimed to avoid "overfitting" and equals to 0.2. For optimization, we applied a weight decay of 0.0001and a learning rate of 0.01. In the output layer, two logistic units to obtain the probabilities of the given sample belonging to either of the two classes were employed. The backpropagation scheme was applied to generate the derivative of the objective function.

$$loss_i = -log\left(\frac{e^{U_K}}{\sum_{d=1}^{L} e^{U_d}}\right) \qquad (5)$$

where $loss_i$ implies the loss value for training data i, U_K demonstrates the raw production score (is not normalized) for the reference class K.

The un-normalized production score is generated by multiplying the outputs from the previous FC layer with the parameters of the corresponding logistic unit. To find the normalized scores for each class between 0 and 1, the denominator aggregates the scores for all the logistic units L. Since two output neurons are presented at the output layer, in the above equation L is equal to 2.

3. Experiments

3.1 Datasets

The proposed novel technique and three recently published models were investigated on a public chest dataset (Yang et al. 2020) to evaluate the reliability, validity, and accuracy of experiments. This dataset is available at https://github.com/UCSD-AI4H/COVID-C. To segment the corrupted tissues accurately, four experienced specialists segmented the borders manually. It is noteworthy that by employing an augmentation strategy to increase the number of data, a lot of new samples are generated. Also, 70% of data for training, 10% for validating, and 20% for testing are used. Data Augmentations are useful approaches to decrease the validation and training error. The augmentation methods artificially inflate the training dataset size by either data oversampling or warping. When in the augmentation process the labels of the existing images are preserved, this process is called data warping augmentations. This method includes augmentations such as color and geometric transformations, adversarial training, random erasing, and neural style transfer. Oversampling augmentations generate synthetic samples and add them to the training set (Bahadur Chandra et al. 2020).

Six approaches of data augmentation are utilized in this paper to increase efficiency, namely Flipping, Color space, Rotation, Translation, Noise injection, Color space transformations, Random erasing.

In the Flipping, a horizontal axis flipping is used. In the Color space, contrast-enhancing is employed. In the Rotation, 180 degrees is selected. In the Translation, left, right, up, and down are applied. In Noise injection, a Gaussian distribution is utilized. In the Color space transformations, decreasing and increasing the pixel values by a constant value are applied. In the Random erasing, an n × m patch of an image is randomly selected and masking it with zero values.

3.2 Evaluation metrics

In this study, the following nine measures were calculated by comparing the segmentation results with that of lesions segmented by the experts to appraise the proposed architecture's efficiency. The promising accuracy of the proposed two-path architecture was assessed using Recall, Precision, F-score, ASD (average surface distance), RVD (relative volume difference), RMSD (root mean square symmetric surface distance), MSD (maximum surface distance), VOE (volume overlap error), and DICE (dice similarity) (Lu et al. 2014; Liao et al. 2016; Suresh, Rao & Reddy 2019; Ranjbarzadeh & Saadi 2020). Some mentioned metrics are defined as follows:

$$\begin{cases} Precision = \dfrac{TP}{TP+FP} \times 100\% & (6) \\ Recall = \dfrac{TP}{TP+FN} \times 100\% & (7) \\ F = \dfrac{2 \times Precision \times \; Recall}{Precision + \; Recall} \times 100\% & (8) \\ DICE = \left(2 \times \dfrac{TP}{2TP+FP+FN}\right) \times 100\% & (9) \\ VOE(M_{s1}, M_{s2}) = \left(1 - \dfrac{M_{s1} \cap M_{s2}}{M_{s1} \cup M_{s2}}\right) \times 100\% & (10) \\ RVD(M_{s1}, M_{s2}) = \left(\dfrac{M_{s1} - M_{s2}}{M_{s2}}\right) \times 100\% & (11) \\ ASD = \dfrac{1}{\left|B_{M_{s1}}\right| + \left|B_{M_{s2}}\right|} \times \left(\sum_{x \epsilon B_{M_{s1}}} d(x, B_{M_{s2}}) + \sum_{y \epsilon B_{M_{s2}}} d(y, B_{M_{s1}})\right) & (12) \end{cases}$$

where M_{s1} and M_{s2} denote the result of segmentation using our strategy and ground-truth mask, respectively. Also, $B_{M_{s1}}$ and $B_{M_{s2}}$ imply the borders result of our segmentation technique and ground-truth image, respectively. Moreover, the FN, FP, and TP represent false negative, false positive, and true positive, respectively (Karimi, Ranjbarzadeh Kondrood & Alizadeh 2017; Xu et al. 2020).

Dice similarity coefficient (DSC) is defined as one for a perfect segmentation and is a statistical tool for measuring the similarity between two sets of data. MSD measures the distance between the border of each segmented object from its corresponding border in the ground-truth image. Measuring the difference between the segmented object and related object in the ground-truth image can be calculated by RVD, in which the positive value implies over-segmentation and the negative value represents the under-segmentation result. It means that the best value is zero that indicates the segmented object is equal to the ground-truth image.

3.3 Experimental Results

Our two-path architecture was implemented in Python, and the experiments were run on an Intel(R) Core(TM)i7- 3.4 GHz + GEFORCE GTX 1080 Ti GPU + 16 Gigabytes of RAM under the windows 10 (64-bit) operating system. The results of our pipeline using 3 distinct input images were appraised utilizing the corresponding ground-truths and reported in Tables 2 and 3. In our dataset samples with a large diversity in the volume of the lesions, and not well-defined border (unclear or blurred margin) have the greatest part of the train, validation, and test samples.

For exemplifying the significance of utilizing the grouping of the LDN encoding approach, Z-Score normalization technique, and CNN framework to accurate estimating borders, Fig. 7 demonstrates the outcomes of our structure (drawn by a green line). The results of our method compared to three other recently published methods are shown in Fig. 7 on a few slices with the intensity inhomogeneity, ambiguous boundaries, heterogeneous appearances, and various infection shapes. Accordingly, it can noticeably be observed that the intensity inhomogeneity and ambiguous boundaries inside the lung due to the infection cause the infected regions are not suitably extracted when the DenseNet201 (Jaiswal et al. 2020), Weakly Supervised Deep Learning

(Hu et al. 2020), and Weakly-Supervised Framework (Wang et al. 2020b) approaches are applied.

As indicated in Fig. 7, segmentation by employing the DenseNet201 (Jaiswal et al. 2020) structure shows the fewest match with the reference data (ground-truth), especially when similar intensity values are encountered near the borders of the infected regions. Weakly Supervised Deep Learning (Hu et al. 2020) is good to recognize the infection boundary when there is much distance (more than 20 pixels) between two lesions but when in the small distance (less than 20 pixels) it performs so poorly and the chance of combining two lesions is highly increased. Also, the DenseNet201 (Jaiswal et al. 2020) method under-segment the infected areas in the most cases, whereas the Weakly Supervised Deep Learning (Hu et al. 2020) and Weakly-Supervised Framework (Wang et al. 2020b) models over-segment with equivalent intensity values. Moreover, such pipelines are more prone to boundary leakage, especially when there are unclear borders among the different kinds of infection progress. To solve this issue, we came up with the idea of employing both local and global features when there are three representations of the infected and non-infected tissues. Our model also has not noteworthy boundary leakage, substantial over-segmentation, or under-segmentation, predominantly in particular sections that are near the white objects. By using the Z-Score normalization and Fuzzy clustering methods, our approach is more capable to enhance the contrast near the border of the lung to obtains more accuracy in the distinction of an infected region and vague border of the lung. Considering the heterogeneous textures, opaque appearance of the infected tissue, misalignment of the infection boundaries, unclear borders, and different dimensions of the infection regions, it is more evident that our pipeline suitably finds a pattern most similar to the infected area, which demonstrates its robust performance under realistic scenarios on countless infection outlines. It worth mentioning that in all methods, the white tissue (pulmonary nodules) near the infected area cannot be properly recognized due to the much similarity between both tissue values. The results may get better if the amount of training data is increased.

The proposed two-path CNN structure achieved a higher segmentation performance than the other three evaluated methods when other representations of the lung images are applied, meaning more substantial features are available to achieve the best distinction between classes. The efficiency of our technique on different CT infected lungs was assessed using the Dice similarity index, as illustrated in Fig. 8. The dice score averages for the segmented infection areas with diverse appearance varied from 80% to 94%. As is shown, the worst result belongs to the DenseNet201 approach with an average of 84%. The result of our approach implies that the appearance, intensity values, and outline of the infected tissue cannot significantly affect the segmentation performance and efficiency.

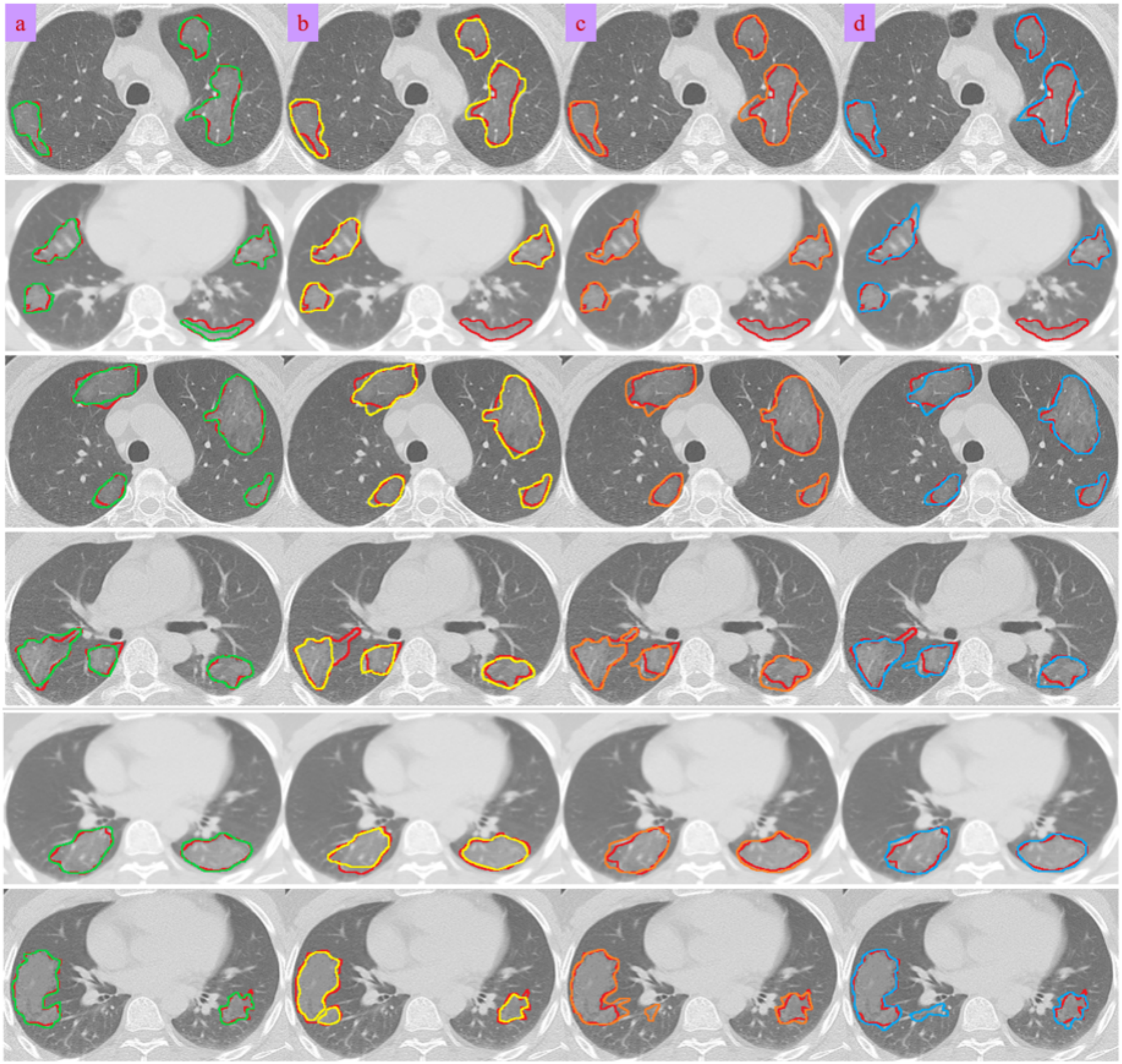

Fig. 7. Comparisons between four different kinds of strategies for COVID-19 Infection Detection. The red contours indicate the reference border (ground-truth). Segmentation based on the (a) Proposed strategy (b) DenseNet201 (Jaiswal et al. 2020), (c) Weakly Supervised Deep Learning (Hu et al. 2020), and (e) Weakly-Supervised Framework (Wang et al. 2020b).

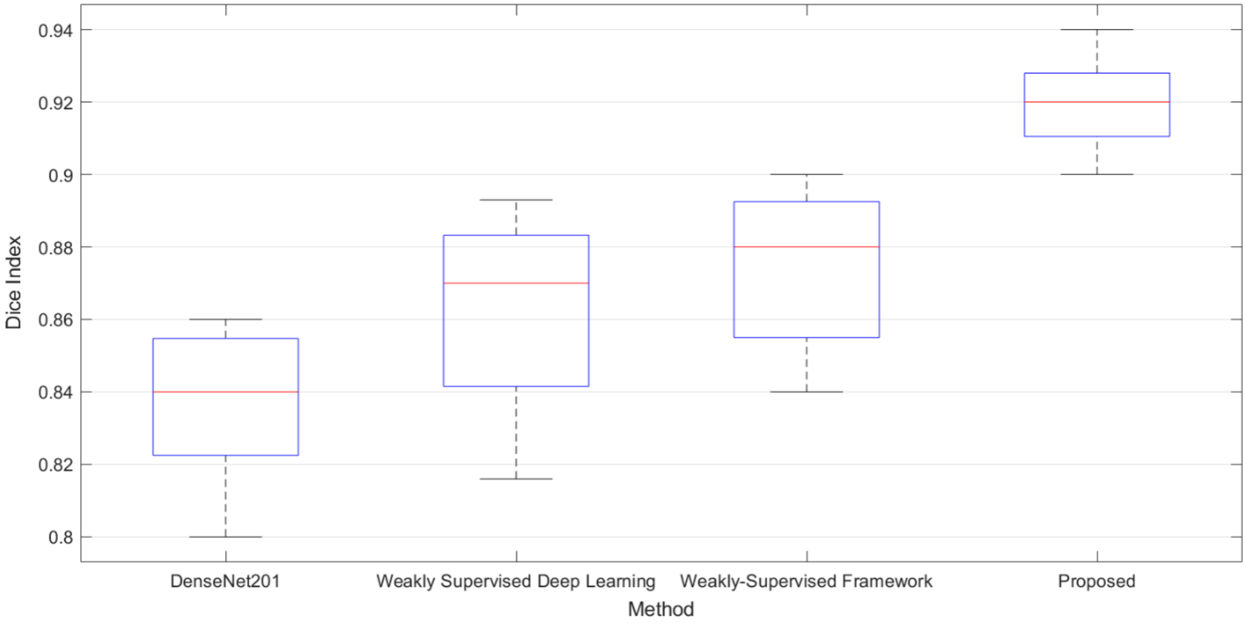

Fig. 8. Comparison between the dice scores of the four model employed for lung infection segmentation in CT images.

Tables 2 and 3 indicate the comprehensive evaluation of our complex strategy for lesions segmenting and compare it with the results of other mentioned methods on our dataset.

Table 2 implies a quantitative comparison, in practice, between the automated lesion segmentation outcomes of the novel proposed two-patch model over the other three mentioned approaches. For each index in tables 2 and 3, the highest values of RVD, ASD, RMS, MSD, VOE, Recall, Precision, and F-score are highlighted in bold. The outcomes of every first five assessment criteria are demonstrated by standard deviation and mean values in Table 2. The proposed two-route segmentation model gains a smaller mean in mentioned assessment criteria. The obtained VOE is meaningfully altered between all appraised architectures, while the outcomes of RMS and ASD imply the lowest variance. The RVD score for DenseNet201, Proposed CNN and Proposed CNN + fuzzy c-mean algorithms are less than 0. Also, adding the LDN method to the proposed CNN model leads to observe the positive value in the RVD result. The RMS score imply that the proposed CNN + fuzzy c-mean + LDN and Proposed CNN + LDN methods produced the best outcomes among the seven structures. Also, the DenseNet201 technique gains the highest mean score of RMS.

In addition, the mean value of MSD and VOE of the models employed by DenseNet201 and Weakly-Supervised Framework were outstandingly higher as compared to our outcomes. Moreover, Both the Weakly Supervised Deep Learning and the Weakly-Supervised Framework models show a large standard deviation in the RVD; however, a major standard deviation in MSD score is obtained in DenseNet201 method. The observed results in the ASD and VOE indicate that adding LDN and Fuzzy clustering methods to our CNN model can significantly improve our model accuracy.

Table 2. Quantitative comparison of infected tissue segmentation outcomes based on our model and three recently published structures. The evaluations are based on average surface distance (ASD), relative volume difference (RVD), Volume overlap error (VOE), root mean square symmetric surface distance (RMS), maximum surface distance (MSD).

approach	**ASD (mm)**	**VOE (%)**	**RVD (%)**	**MSD (mm)**	**RMS (mm)**
DenseNet201 (Jaiswal et al. 2020)	5.4±0.3	11.4±7.3	-4.2±5.9	23.6±7.1	5.9±0.4
Weakly Supervised Deep Learning (Hu et al. 2020)	5.1±0.4	11±7.3	7.8±10.3	21±6.6	5.5±0.7
Weakly-Supervised Framework (Wang et al. 2020b)	6.1±0.6	11.7±4.2	8.3±6.6	22.7±5.2	5.8±0.5
Proposed CNN	6.3±0.5	11.9±6.8	-5.8±3.5	21.3±6.1	5.7±0.4
Proposed CNN + LDN	5.1±0.1	8.3±4.7	6.5±4.1	15.4±4.8	4.7±0.2
Proposed CNN + fuzzy c-mean	5.5.3±0.4	8.9±5.2	-6.9±7.3	16.5±4.9	5.2±0.5
Proposed CNN + fuzzy c-mean + LDN	**2.8±0.3**	**5.6±1.2**	**3.7±5.6**	**7.4±7.3**	**3.6±0.2**

Table 3. Quantitative comparison of infected tissue segmentation outcomes based on our pipeline and three recently published structures. The evaluations are based on Recall, Precision, F-score.

approach	Precision(%)	Recall(%)	F-score
DenseNet201 (Jaiswal et al. 2020)	86%	89%	87%
Weakly Supervised Deep Learning (Hu et al. 2020)	88%	90%	89%
Weakly-Supervised Framework (Wang et al. 2020b)	91%	89%	90%
Proposed CNN	88%	89%	88%
Proposed CNN + LDN	93%	91%	92%
Proposed CNN + fuzzy c-mean	92%	94%	93%
Proposed CNN + fuzzy c-mean + LDN	**96%**	**97%**	**97%**

The results in Table 3, indicate the measurements for differentiating the objects inside the lung, including normal and infected tissues. As can be observed in Table 3, our technique, CNN + fuzzy c-mean + LDN, consistently performs the best among all approaches. The F-score, Precision, and Recall of the DenseNet201 and Weakly Supervised Deep Learning structures are highly similar to the proposed CNN algorithm; however, by adding the LDN or Fuzzy clustering approach, these three criteria are highly increased. Also, the DenseNet201 approach gains the worst results and our architecture obtains the competitive performance on lesions segmentation in all evaluation metrics.

4. Discussion and Conclusions

In this study, we implemented a two-path CNN pipeline that incorporates the three distinct input images, to automatically segment the infected tissues inside the lung caused due to the COVID-19 from CT images. For a better demonstration of the tissues to extract more key features inside the CNN model, we showed the input CT image represented in the two other different ways which each of them includes some unique information. Due to inflammation inside the lung because of the COVID-19, infected areas near the border of the lung are highly difficult to segment. So, our algorithm first employed a Z-Score normalization technique to obtain a more distinguishable lung border from the original image. Then, by using a fuzzy clustering method, all tissues in the image are clustered and obtain a distinct pixel value for all pixels corresponding to each cluster. This approach helps the CNN pipeline for decreasing the convolutional layers for extracting some key features and leads to a drop in the training time of the pipeline and increase the final efficiency.

Then, an LDN encoding approach was implemented for representing the information of the images in another form to extract more essential details from the input image. This strategy roots in the fact that sometimes by changing the representation domain (like frequency domain rather than the time domain) some other substantial features can be observed.

We also represented a new two-route CNN model that considered semi-global and local information to categorize each pixel in the input image to one of the two normal and infected tissues. The number of the convolutional layers in the global route is more than the local route, while the kernel size for all convolutional layers is the same. To overcome the overfitting problems and boost efficiency, using data augmentation methods the number of samples has been increased. Lastly, using the CT image and two obtained images, our CNN structure was trained.

The suggested two-route segmentation pipeline was appraised on a public dataset which 70% of data for training, 10% for validating, and 20% for testing were used. Our significant findings demonstrate that our CNN pipeline and three distinct input images gained the following: 1) acceptable performance even if the infected area shared an extended border with touching tissues, 2) appropriately robust as indicated by the negligible standard deviations which show the uniformity of the values for all the nine criteria and 3) accomplished well in the detection and segmentation process even for the intricate cases with numerous unalike categories of the infection, which had the amoeboid shapes and analogous thicknesses.

The proposed architecture satisfactorily overcomes the difficulty of failing in accurate detection of the lesions at the presence of the similar adjacent tissues and identification of an uneven border where is seemed not properly appear to exist with an aim to reach superior outcomes. In addition, the employed technique does not require more extra parameters for feeding into the algorithm apart from one CT image to define the position of the lesions and border detection. But the functional limitation of this architecture is that the white matter (pulmonary nodules) inside the normal lung near the border of a lesion cannot properly be recognized from the infected tissue. We think that by increasing the training samples this problem can be solved.

Tables 2 and 3 approve that our technique divides erratic and wide infections and irregular shapes. Most of the segmentation strategies that merely rely on measuring the illumination, energy, thickness, location, and shape could fail when the infected tissue and other touching objects have an analogous density and intensity levels. Under such specific circumstances, applying additional distinguishable features from different kinds of images may result in improving the ability of segmentation and fulfilled a leading role in gently separating infections associated with the above-mentioned problems. Our unique pipeline could potentially be more advantageous when encountering diverse infections with the blurred boundaries and wide-ranging lesion sizes. The implemented procedure proposed herein yields a more classification efficiency in terms of simplicity, stability, and time consumption compared to the baseline models.

Acknowledgement

None. No funding to declare.

References:

Ahmadi, M., Sharifi, A., Dorosti, S., Jafarzadeh Ghoushchi, S. & Ghanbari, N. 2020. Investigation of effective climatology parameters on COVID-19 outbreak in Iran. *Science of the Total Environment* 729: 138705.

Ali, W.A., Manasa, K.N., Bendechache, M., Aljunaid, M.F. & Sandhya, P. 2020. A review of current machine learning approaches for anomaly detection in network traffic. Telecommunications Association Inc.

Ardakani, A.A., Kanafi, A.R., Acharya, U.R., Khadem, N. & Mohammadi, A. 2020. Application of deep learning technique to manage COVID-19 in routine clinical practice using CT images: Results of 10 convolutional neural networks. *Computers in Biology and Medicine* 121: 103795.

de Assis Neto, S.R., Santos, G.L., da Silva Rocha, E., Bendechache, M., Rosati, P., Lynn, T. & Takako Endo, P. 2020. Detecting Human Activities Based on a Multimodal Sensor Data Set Using a Bidirectional Long Short-Term Memory Model: A Case Study. *Studies in Systems, Decision and Control*, hlm. 31–51. Springer.

Azary, H. & Abdoos, M. 2020. A Semi-supervised method for tumor segmentation in mammogram images. *Journal of Medical Signals and Sensors* 10(1): 12–18.

Bahadur Chandra, T., Verma, K., Kumar Singh, B., Jain, D. & Singh Netam, S. 2020. Coronavirus Disease (COVID-19) Detection in Chest X-Ray Images using Majority Voting Based Classifier Ensemble. *Expert Systems with Applications*: 113909.

Barstugan, M., Ozkaya, U. & Ozturk, S. 2020. Coronavirus (COVID-19) Classification using CT Images by Machine Learning Methods.

Bendechache, M. 2019. Study of Distributed Dynamic Clustering Framework for Spatial Data Mining.

Bendechache, M. & Kechadi, M.T. 2015. Distributed clustering algorithm for spatial data mining. *ICSDM 2015 - Proceedings 2015 2nd IEEE International Conference on Spatial Data Mining and Geographical Knowledge Services*, hlm. 60–65. Institute of Electrical and

Electronics Engineers Inc.

Bendechache, M., Kechadi, M.T. & Le-Khac, N.A. 2016. Efficient large scale clustering based on data partitioning. *Proceedings - 3rd IEEE International Conference on Data Science and Advanced Analytics, DSAA 2016*, hlm. 612–621. Institute of Electrical and Electronics Engineers Inc.

Bendechache, M., Le-Khac, N.A. & Kechadi, M.T. 2016. Hierarchical Aggregation Approach for Distributed Clustering of Spatial Datasets. *IEEE International Conference on Data Mining Workshops, ICDMW*, hlm. 1098–1103. IEEE Computer Society.

Bengio, Y. 2012. Practical Recommendations for Gradient-Based Training of Deep Architectures. hlm. 437–478. Springer, Berlin, Heidelberg.

Calik, N., Belen, M.A. & Mahouti, P. 2020. Deep learning base modified MLP model for precise scattering parameter prediction of capacitive feed antenna. *International Journal of Numerical Modelling: Electronic Networks, Devices and Fields* 33(2).

Di Cataldo, S. & Ficarra, E. 2017. Mining textural knowledge in biological images: Applications, methods and trends. Elsevier B.V.

Chen, J., Liu, Z., Wang, H., Nunez, A. & Han, Z. 2018. Automatic defect detection of fasteners on the catenary support device using deep convolutional neural network. *IEEE Transactions on Instrumentation and Measurement* 67(2): 257–269.

Chen, J., Wu, L., Zhang, J., Zhang, L., Gong, D., Zhao, Y., Hu, S., Wang, Y., Hu, X., Zheng, B., Zhang, K., Wu, H., Dong, Z., Xu, Y., Zhu, Y., Chen, X., Yu, L. & Yu, H. 2020. Deep learning-based model for detecting 2019 novel coronavirus pneumonia on high-resolution computed tomography: a prospective study. *medRxiv*: 2020.02.25.20021568.

Dhanachandra, N. & Chanu, Y.J. 2020. An image segmentation approach based on fuzzy c-means and dynamic particle swarm optimization algorithm. *Multimedia Tools and Applications* 79(25–26): 18839–18858.

Doğantekin, A., Özyurt, F., Avcı, E. & Koç, M. 2019. A novel approach for liver image classification: PH-C-ELM. *Measurement: Journal of the International Measurement Confederation* 137: 332–338.

Dolz, J., Desrosiers, C. & Ben Ayed, I. 2018. 3D fully convolutional networks for subcortical segmentation in MRI: A large-scale study. *NeuroImage* 170: 456–470.

Dong, N., Kampffmeyer, M., Liang, X., Wang, Z., Dai, W. & Xing, E. 2018. Reinforced auto-zoom net: Towards accurate and fast breast cancer segmentation in whole-slide images. *Lecture Notes in Computer Science (including subseries Lecture Notes in Artificial Intelligence and Lecture Notes in Bioinformatics)*, hlm. 317–325. Springer Verlag.

Dorosti, S., Jafarzadeh Ghoushchi, S., Sobhrakhshankhah, E., Ahmadi, M. & Sharifi, A. 2020. Application of gene expression programming and sensitivity analyses in analyzing effective parameters in gastric cancer tumor size and location. *Soft Computing* 24(13): 9943–9964.

Dureja, A. & Pahwa, P. 2018. Analysis of Non-Linear Activation Functions for Classification Tasks Using Convolutional Neural Networks. *Recent Patents on Computer Science* 12(3):

156–161.

Dvornik, N., Mairal, J. & Schmid, C. 2019. On the Importance of Visual Context for Data Augmentation in Scene Understanding. *IEEE Transactions on Pattern Analysis and Machine Intelligence*.

Ettensperger, F. 2020. Comparing supervised learning algorithms and artificial neural networks for conflict prediction: performance and applicability of deep learning in the field. *Quality and Quantity* 54(2): 567–601.

Fan, D.P., Zhou, T., Ji, G.P., Zhou, Y., Chen, G., Fu, H., Shen, J. & Shao, L. 2020. Inf-Net: Automatic COVID-19 Lung Infection Segmentation From CT Images. *IEEE transactions on medical imaging* 39(8): 2626–2637.

Friedman, L. & Komogortsev, O. V. 2019. Assessment of the Effectiveness of Seven Biometric Feature Normalization Techniques. *IEEE Transactions on Information Forensics and Security* 14(10): 2528–2536.

Ghoushchi, S.J., Gharibi, K., Osgooei, E., Ab Rahman, M.N. & Khazaeili, M. 2020. Risk Prioritization in Failure Mode and Effects Analysis with Extended SWARA and MOORA Methods Based on Z-Numbers Theory. *Informatica* 0(0): 1–27.

Hamzenejad, A., Ghoushchi, S.J., Baradaran, V. & Mardani, A. 2020. A robust algorithm for classification and diagnosis of brain disease using local linear approximation and generalized Autoregressive Conditional Heteroscedasticity model. *Mathematics* 8(8): 1268.

Hassantabar, S., Ahmadi, M. & Sharifi, A. 2020. Diagnosis and detection of infected tissue of COVID-19 patients based on lung x-ray image using convolutional neural network approaches. *Chaos, Solitons and Fractals* 140: 110170.

Havaei, M., Davy, A., Warde-Farley, D., Biard, A., Courville, A., Bengio, Y., Pal, C., Jodoin, P.M. & Larochelle, H. 2017. Brain tumor segmentation with Deep Neural Networks. *Medical Image Analysis* 35: 18–31.

He, K., Zhang, X., Ren, S. & Sun, J. 2016a. Deep Residual Learning for Image Recognition.

He, T., Huang, W., Qiao, Y. & Yao, J. 2016b. Text-Attentional Convolutional Neural Network for Scene Text Detection. *IEEE Transactions on Image Processing* 25(6): 2529–2541.

Hu, S., Gao, Y., Niu, Z., Jiang, Y., Li, L., Xiao, X., Wang, M., Fang, E.F., Menpes-Smith, W., Xia, J., Ye, H. & Yang, G. 2020. Weakly Supervised Deep Learning for COVID-19 Infection Detection and Classification from CT Images. *IEEE Access* 8: 118869–118883.

Islam, M.Z., Islam, M.M. & Asraf, A. 2020. A combined deep CNN-LSTM network for the detection of novel coronavirus (COVID-19) using X-ray images. *Informatics in Medicine Unlocked* 20: 100412.

Jafarzadeh-Ghoushchi, S. & Rahman, M.N.A. 2016. Performance study of artificial neural network modelling to predict carried weight in the transportation system. *International Journal of Logistics Systems and Management* 24(2): 200–212.

Jafarzadeh Ghoushchi, S., Ab Rahman, M.N., Raeisi, D., Osgooei, E. & Jafarzadeh Ghoushji, M.

2020. Integrated Decision-Making Approach Based on SWARA and GRA Methods for the Prioritization of Failures in Solar Panel Systems under Z-Information. *Symmetry* 12(2): 310.

Jaiswal, A., Gianchandani, N., Singh, D., Kumar, V. & Kaur, M. 2020. Classification of the COVID-19 infected patients using DenseNet201 based deep transfer learning. *Journal of Biomolecular Structure and Dynamics*: 1–8.

Kamble, B., Sahu, S.P. & Doriya, R. 2020. A review on lung and nodule segmentation techniques. *Lecture Notes in Networks and Systems*, hlm. 555–565. Springer.

Karimi, N., Ranjbarzadeh Kondrood, R. & Alizadeh, T. 2017. An intelligent system for quality measurement of Golden Bleached raisins using two comparative machine learning algorithms. *Measurement: Journal of the International Measurement Confederation* 107: 68–76.

Khond, S.V. 2020. Effect of Data Normalization on Accuracy and Error of Fault Classification for an Electrical Distribution System. *Smart Science*.

Krizhevsky, A., Sutskever, I. & Hinton, G.E. 2012. ImageNet Classification with Deep Convolutional Neural Networks.

Leng, C., Zhang, H., Li, B., Cai, G., Pei, Z. & He, L. 2019. Local Feature Descriptor for Image Matching: A Survey. *IEEE Access* 7: 6424–6434.

Liao, M., Zhao, Y. qian, Wang, W., Zeng, Y. zhan, Yang, Q., Shih, F.Y. & Zou, B. ji. 2016. Efficient liver segmentation in CT images based on graph cuts and bottleneck detection. *Physica Medica* 32(11): 1383–1396.

Liu, F., Lin, G. & Shen, C. 2015. CRF learning with CNN features for image segmentation. *Pattern Recognition* 48(10): 2983–2992.

Liu, L., Lao, S., Fieguth, P.W., Guo, Y., Wang, X. & Pietikäinen, M. 2016. Median Robust Extended Local Binary Pattern for Texture Classification. *IEEE Transactions on Image Processing* 25(3): 1368–1381.

Liu, Z., Song, Y.Q., Sheng, V.S., Wang, L., Jiang, R., Zhang, X. & Yuan, D. 2019. Liver CT sequence segmentation based with improved U-Net and graph cut. *Expert Systems with Applications* 126: 54–63.

Lu, X., Wu, J., Ren, X., Zhang, B. & Li, Y. 2014. The study and application of the improved region growing algorithm for liver segmentation. *Optik* 125(9): 2142–2147.

Luo, Y.T., Zhao, L.Y., Zhang, B., Jia, W., Xue, F., Lu, J.T., Zhu, Y.H. & Xu, B.Q. 2016. Local line directional pattern for palmprint recognition. *Pattern Recognition* 50: 26–44.

Mahmood, A., Bennamoun, M., An, S., Sohel, F., Boussaid, F., Hovey, R., Kendrick, G. & Fisher, R.B. 2017. Deep Learning for Coral Classification. *Handbook of Neural Computation*, hlm. 383–401. Elsevier Inc.

Minaee, S., Kafieh, R., Sonka, M., Yazdani, S. & Jamalipour Soufi, G. 2020. Deep-COVID: Predicting COVID-19 from chest X-ray images using deep transfer learning. *Medical Image Analysis* 65: 101794.

Naiemi, F., Ghods, V. & Khalesi, H. 2021. A novel pipeline framework for multi oriented scene text image detection and recognition. *Expert Systems with Applications* 170: 114549.

Nasir, T., Asmael, M., Zeeshan, Q. & Solyali, D. 2020. Applications of Machine Learning to Friction StirWelding Process Optimization. *Jurnal Kejuruteraan* 32(1).

Nour, M., Cömert, Z. & Polat, K. 2020. A Novel Medical Diagnosis model for COVID-19 infection detection based on Deep Features and Bayesian Optimization. *Applied Soft Computing Journal*: 106580.

Ouyang, X., Huo, J., Xia, L., Shan, F., Liu, J., Mo, Z., Yan, F., Ding, Z., Yang, Q., Song, B., Shi, F., Yuan, H., Wei, Y., Cao, X., Gao, Y., Wu, D., Wang, Q. & Shen, D. 2020. Dual-Sampling Attention Network for Diagnosis of COVID-19 From Community Acquired Pneumonia. *IEEE transactions on medical imaging* 39(8): 2595–2605.

Rajinikanth, V., Dey, N., Raj, A.N.J., Hassanien, A.E., Santosh, K.C. & Raja, N.S.M. 2020. Harmony-Search and Otsu based System for Coronavirus Disease (COVID-19) Detection using Lung CT Scan Images.

Ranjbarzadeh, R. & Baseri Saadi, S. 2020. Corrigendum to "Automated liver and tumor segmentation based on concave and convex points using fuzzy c-means and mean shift clustering" (Measurement (2020) 150, (S0263224119309522), (10.1016/j.measurement.2019.107086)). *Measurement: Journal of the International Measurement Confederation* 151.

Ranjbarzadeh, R., Baseri Saadi, S. & Amirabadi, A. 2020. LNPSS: SAR Image Despeckling Based on Local and Non-Local Features Using Patch Shape Selection and Edges linking. *Measurement* 164: 107989.

Ranjbarzadeh, R. & Saadi, S.B. 2020. Automated liver and tumor segmentation based on concave and convex points using fuzzy c-means and mean shift clustering. *Measurement: Journal of the International Measurement Confederation* 150.

Ranjbarzadeh, R., Saadi, S.B. & Amirabadi, A. 2020. LNPSS: SAR image despeckling based on local and non-local features using patch shape selection and edges linking. *Measurement: Journal of the International Measurement Confederation* 164.

Rouhi, R., Jafari, M., Kasaei, S. & Keshavarzian, P. 2015a. Benign and malignant breast tumors classification based on region growing and CNN segmentation. *Expert Systems with Applications* 42(3): 990–1002.

Rouhi, R., Jafari, M., Kasaei, S. & Keshavarzian, P. 2015b. Benign and malignant breast tumors classification based on region growing and CNN segmentation. *Expert Systems with Applications* 42(3): 990–1002.

Rubin, G.D., Ryerson, C.J., Haramati, L.B., Sverzellati, N., Kanne, J.P., Raoof, S., Schluger, N.W., Volpi, A., Yim, J.J., Martin, I.B.K., Anderson, D.J., Kong, C., Altes, T., Bush, A., Desai, S.R., Goldin, J., Goo, J.M., Humbert, M., Inoue, Y., Kauczor, H.U., Luo, F., Mazzone, P.J., Prokop, M., Remy-Jardin, M., Richeldi, L., Schaefer-Prokop, C.M., Tomiyama, N., Wells, A.U. & Leung, A.N. 2020. The Role of Chest Imaging in Patient Management During the COVID-19 Pandemic: A Multinational Consensus Statement From the Fleischner Society. *Chest* 158(1): 106–116.

Schmidt-Hieber, J. 2020. Nonparametric regression using deep neural networks with ReLU activation function. *Annals of Statistics* 48(4): 1875–1897.

Shan, F., Gao, Y., Wang, J., Shi, W., Shi, N., Han, M., Xue, Z., Shen, D. & Shi, Y. 2020. Lung Infection Quantification of COVID-19 in CT Images with Deep Learning.

Shi, F., Wang, J., Shi, J., Wu, Z., Wang, Q., Tang, Z., He, K., Shi, Y. & Shen, D. 2020. Review of Artificial Intelligence Techniques in Imaging Data Acquisition, Segmentation and Diagnosis for COVID-19. *IEEE Reviews in Biomedical Engineering*.

Suresh, R., Rao, A.N. & Reddy, B.E. 2019. Detection and classification of normal and abnormal patterns in mammograms using deep neural network. *Concurrency and Computation: Practice and Experience* 31(14).

Torres, A.D., Yan, H., Aboutalebi, A.H., Das, A., Duan, L. & Rad, P. 2018. Patient facial emotion recognition and sentiment analysis using secure cloud with hardware acceleration. *Computational Intelligence for Multimedia Big Data on the Cloud with Engineering Applications*, hlm. 61–89. Elsevier.

Tuncer, T., Dogan, S. & Ozyurt, F. 2020. An automated Residual Exemplar Local Binary Pattern and iterative ReliefF based corona detection method using lung X-ray image. *Chemometrics and Intelligent Laboratory Systems* 203: 104054.

Ucar, F. & Korkmaz, D. 2020. COVIDiagnosis-Net: Deep Bayes-SqueezeNet based diagnosis of the coronavirus disease 2019 (COVID-19) from X-ray images. *Medical Hypotheses* 140: 109761.

Uddin, M.Z., Hassan, M.M., Almogren, A., Zuair, M., Fortino, G. & Torresen, J. 2017. A facial expression recognition system using robust face features from depth videos and deep learning. *Computers and Electrical Engineering* 63: 114–125.

Wahab, N., Khan, A. & Lee, Y.S. 2017. Two-phase deep convolutional neural network for reducing class skewness in histopathological images based breast cancer detection. *Computers in Biology and Medicine* 85: 86–97.

Waleed Salehi, A., Baglat, P. & Gupta, G. 2020. Review on Machine and Deep Learning Models for the Detection and Prediction of Coronavirus. *Materials Today: Proceedings*.

Wang, G., Liu, X., Li, C., Xu, Z., Ruan, J., Zhu, H., Meng, T., Li, K., Huang, N. & Zhang, S. 2020a. A Noise-Robust Framework for Automatic Segmentation of COVID-19 Pneumonia Lesions from CT Images. *IEEE Transactions on Medical Imaging* 39(8): 2653–2663.

Wang, X., Deng, X., Fu, Q., Zhou, Q., Feng, J., Ma, H., Liu, W. & Zheng, C. 2020b. A Weakly-Supervised Framework for COVID-19 Classification and Lesion Localization From Chest CT. *IEEE Transactions on Medical Imaging* 39(8): 2615–2625.

Willner, M., Fior, G., Marschner, M., Birnbacher, L., Schock, J., Braun, C., Fingerle, A.A., Noël, P.B., Rummeny, E.J., Pfeiffer, F. & Herzen, J. 2015. Phase-Contrast Hounsfield Units of Fixated and Non-Fixated Soft-Tissue Samples. *PLOS ONE* 10(8): e0137016.

Xu, X., Jiang, X., Ma, C., Du, P., Li, X., Lv, S., Yu, L., Ni, Q., Chen, Y., Su, J., Lang, G., Li, Y., Zhao, H., Liu, J., Xu, K., Ruan, L., Sheng, J., Qiu, Y., Wu, W., Liang, T. & Li, L. 2020. A Deep Learning System to Screen Novel Coronavirus Disease 2019 Pneumonia. *Engineering*.

Yang, X., He, X., Zhao, J., Zhang, Y., Zhang, S. & Xie, P. 2020. COVID-CT-Dataset: A CT Scan Dataset about COVID-19. *arXiv*.

Yin, W., Schütze, H., Xiang, B. & Zhou, B. 2016. ABCNN: Attention-Based Convolutional Neural Network for Modeling Sentence Pairs. *Transactions of the Association for Computational Linguistics* 4: 259–272.

Zhong, J., Liu, Z., Han, Z., Han, Y. & Zhang, W. 2019. A CNN-Based Defect Inspection Method for Catenary Split Pins in High-Speed Railway. *IEEE Transactions on Instrumentation and Measurement* 68(8): 2849–2860.

Zhou, L., Li, Z., Zhou, J., Li, H., Chen, Y., Huang, Y., Xie, D., Zhao, L., Fan, M., Hashmi, S., Abdelkareem, F., Eiada, R., Xiao, X., Li, L., Qiu, Z. & Gao, X. 2020. A Rapid, Accurate and Machine-Agnostic Segmentation and Quantification Method for CT-Based COVID-19 Diagnosis. *IEEE Transactions on Medical Imaging* 39(8): 2638–2652.